A Comparative Study of Artificial Neural Network Approach for Autonomous Robot's TTC Prediction

Imane Arrouch, Junita Mohamad Saleh, Patrick Goh, and Nur Syazreen Ahmad*
School of Electrical & Electronic Engineering, Universiti Sains Malaysia, 14300 Nibong Tebal, Penang, Malaysia.
Email: *Corresponding author: syazreen@usm.my

***Abstract*—In this study, the focus is on close proximity Time-to-Collision (TTC) prediction from an Autonomous Robot (AR)'s perception system, which is built with an X-band Doppler radar for relative speed estimation and infrared proximity sensors for direction and distance sensing from a moving obstacle. To compensate for the possibility of poor ranging performance, an Artificial Neural Network (ANN) approach is introduced to enhance prediction accuracy. A comparative performance analysis against conventional and Linear Regression (LR) methods was also conducted and results demonstrated that the predicted TTC with the ANN model trained with the Levenberg-Marquardt algorithm successfully reduced the average error to 0.155s, which was a considerable 50% reduction from the conventional method.**

***Index Terms*—artificial neural network, time-to-collision, doppler radar, autonomous robot**

I. INTRODUCTION

Autonomous navigation with mobile robotics has been an active area of research since the past two decades [1]-[3]. Collision avoidance strategy is one crucial feature in most Autonomous Robots (ARs) to ensure safe maneuvering, particularly in unknown or cluttered environments. Unlike many traditional collision avoidance methods which convert the distance from an obstacle into a binary decision, the Time-to-Collision (TTC) information allows for a more reliable judgement as it also indicates the probability of collision even when the obstacle is detected beyond the robot's safety radius.

TTC is calculated by dividing the difference between two distance measurements by the rate of change in that range. Ultrasonic sensors, infrared (IR) proximity sensors, cameras, laser rangefinders, and radars are examples of on-board sensors that are often employed for distance measuring in mobile robotics [4]. Ultrasonic sensors calculate the distance from an object using the Time-of-Flight (ToF) of the sonic wave, which is calculated from the moment it is released until the echo is returned. The accuracy of these sensors is not affected by colours and types of materials or environmental lighting, but due to their medium-sized Field of View (FoV) on the azimuth plane which is approximately 30°, an array of these sensors in the form of a ring with overlapping FoVs is typically required to detect the obstacle's direction [5]. In comparison, IR proximity sensors have a much smaller FoV and produce distance measurements at a much faster rate, but a large number of these sensors are needed to provide full coverage of the robot's path. Plus, because they work on the principle of reflected light waves, their precision is affected by both ambient lighting and the reflectivity of the item. Laser rangefinders, on the other hand, can calculate the distance with far better precision utilizing the ToF measurement of pulsed light emitted from a laser beam, but they are usually much more expensive and may not be suitable for human coexisting environments due to eye-safety concerns. Laser rangefinders, like IR sensors, are vulnerable to visual disturbances, and both may have difficulties in estimating the relative speed between the robot and a moving obstacle [6].

Compared to cameras, laser- and IR-based sensors, immunity to environmental conditions and ambient lighting is a remarkable benefit of radar-based sensors. Continuous-wave Doppler radar for instance relies on Doppler effect to detect a moving object at a distance, and it is generally used to estimate the object's speed without requiring the Line-of-Sight (LoS) visibility. X-Band Doppler radars are low-cost, specialized radars that operate at a frequency between 8 and 12Ghz. Their radiation power levels are typically low enough to avoid potential radiation hazards to the surrounding [7]. A comparative study in [8] has shown that the X-band-type radar is more suited for collision avoidance with ARs or unmanned vehicles due to its ability to provide good performance and angular accuracy in short-range moving obstacle detections.

Despite their benefits, X-band Doppler radars are rarely used for TTC prediction due to their distance measurement inaccuracy [9]. In addition, its radiation which covers nearly 80% of its front view prevents it from determining the direction of the moving obstacle. While there have been advances in forecasting TTC using camera-based approaches, the computation for an obstacle approaching non-parallel to the subject's LoS remains difficult [10]. To reduce the effects of motion blur which amplify when the obstacle is sufficiently close to the subject, a sensor fusion

Manuscript received December 4, 2021; revised March 1, 2022.

doi: 10.18178/ijmerr.11.5.345-350

approach combining an IR- or radar-based sensor and a camera can offer a solution but at the price of higher cost, complexity, and computational load [11], [12], and the majority of known methods are mostly devoted to tracking the position of obstacles and estimating the likelihood of imminent head-on collision situations, with a focus on pedestrian egocentric navigation systems [13], [14].

In this work, the focus is on close proximity TTC prediction from an AR's perception system. The proposed TTC prediction method utilizes an X-band Doppler radar for relative speed estimation and IR proximity sensors for direction and distance sensing from a moving obstacle. To compensate for the possibility of poor ranging performance, an Artificial Neural Network (ANN) approach is introduced to enhance prediction accuracy. A comparative performance analysis against conventional and Linear Regression (LR) methods was also conducted and results showed that the predicted TTC with the ANN model successfully reduced the average error to 0.1s, which was a considerable 50% reduction from the conventional method.

II. Methodology

A. Autonomous Robot (AR) and Sensors

In this work, an AR's perception system for TTC prediction was developed using a single X-Band Doppler radar and five IR proximity sensors. The radar's vertical and horizontal 3dB beam widths are 36°, and 72° respectively, and its working voltage is 5±0.25V. Fig. 1 illustrates the positions of the sensors with respect to the AR where the antenna patches of the radar were positioned facing the robot's front side while the IR sensors were placed equidistant from each other at the robot's front edge. This configuration would create a perception model with a detection area as depicted in Fig. 2 where the radiation pattern of the radar is represented by the yellow curve. The proximity sensors on the other hand have a narrow band as represented by the blue beams which were designed to have a good detection accuracy within 0.2-1.5m range.

Fig. 3 illustrates the processing stages within the radar module where the Doppler shift which is the output from the mixer is generated when there is a difference in the received frequency, f_r, and the transmitted frequency, f_t which is set at 10.525 GHz. As the amplitude is in μV, a signal conditioning amplifier is used to amplify the signal to a processable level.

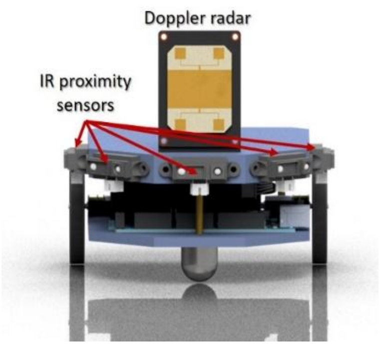

Figure 1. The AR's prototype with on-board Doppler radar and proximity sensor.

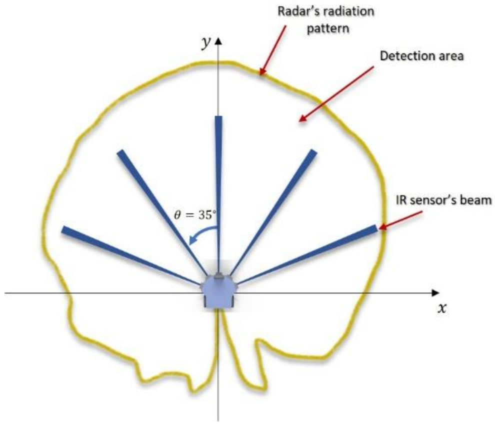

Figure 2. Illustration on the AR's detection area on the azimuth plane.

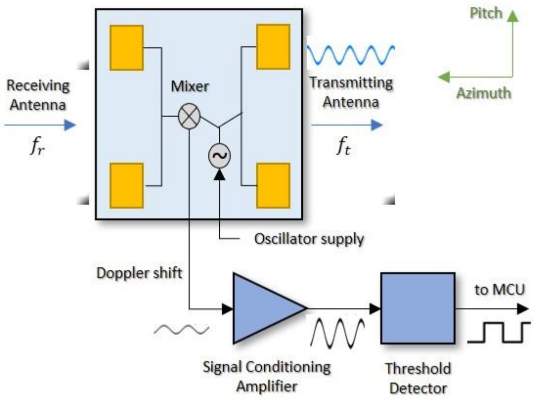

Figure 3. Doppler radar module description. The yellow squares denote the antenna patches.

The amplified signal is then passed through a threshold detector to produce digital pulses which will be further processed by the microcontroller (MCU). As the velocity of motion is proportional to the frequency of Doppler shift, it can be calculated using the following Doppler equation $v = (c \times f_d)/(2 \times f_t \times \cos\alpha)$ where f_d refers to the Doppler frequency, c is the speed of light (i.e., 3×10^8m/s), and α is the angle between the target moving direction and the vertical axis of the module. Since this work only considers obstacles on the same level as the subject (i.e., on the ground), the angle can be assumed sufficiently small, so we will have $\cos\alpha \to 1$, and

$$v = \frac{c \times f_d}{2 \times f_t} = \underbrace{\left(\frac{c}{2f_t}\right)}_{\beta} f_d \tag{1}$$

Hence β is a constant (in m) which can be calculated as $\beta = (3 \times 10^8)/(2 \times 10.525 \times 10^9) = 0.0143$. Thus, v (in cm/s) simplifies to $1.43f_d$.

The proximity sensors are placed at $\theta = 0°, \pm35°, \pm70°$ where θ denotes the angle measured from the subject's front view. The focus of this work is on predicting the TTC using the processed signals from the radar and proximity sensors as described above with an ANN approach for collision risk judgement purposes.

B. TTC Estimation

With the perception model as described in the previous section, the TTC can only be measured once the obstacle has entered the subject's detection area, and it can be theoretically calculated as follows:

$$TTC = \frac{r}{\Delta V} = \frac{r}{V_0 - V_s} \tag{2}$$

where r is the actual Euclidean distance from the subject to the obstacle, ΔV is the relative speed between the subject and the obstacle, V_s is the subject's velocity and V_0 is the obstacle's velocity. The TTC can be estimated by using the speed estimated from the Doppler radar, v_r, and distance estimated from the proximity sensor, $\hat{r}$, i.e.

$$\tau_x = \frac{\hat{r}}{v_r} \tag{3}$$

The next section provides an overview of the TTC prediction methods with ANN.

C. TTC Prediction with ANN

An overview of the ANN technique is depicted in Fig. 4 where a feed-forward neural network was constructed with input neurons (denoted by the red square nodes) in the first layer, hidden neurons (denoted by the white nodes) in the middle layer, and a single neuron (represented by the blue node) in the output layer.

The input neurons will be fed with the parameter $x = (x_1, x_2)$ where $x_1 = \tau_x$ (the estimated TTC as described in (3)) and $x_2 = \hat{r}$ (distance obtained from the proximity sensor). The ANN will return the predicted TTC at the output node as follows:

$$\tau_{nn} = \sum_{i=1}^{q} w_{1i}^2 \, y_i + w_0 \tag{4}$$

where q is the number of hidden neurons, w_{1i}^2 is the weight connecting the hidden neuron's output, y_i and the output neuron, and w_0 is the bias at the output layer.

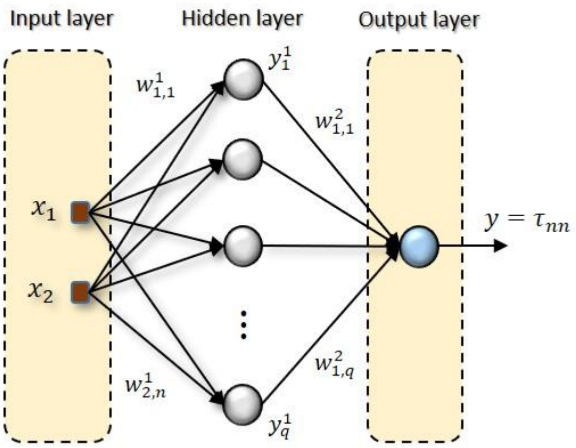

Figure 4. A three-layer ANN with multiple hidden neurons.

To simulate the behavior of biological neurons, each neuron in the hidden layer is constructed with a logarithmic activation function as follows:

$$\phi(\sigma) = \frac{1}{1 + e^{-\sigma}} \tag{5}$$

Thus, in the hidden layer, the output of each neuron can be expressed as

$$y_i = \phi\left(\sum_{j=1}^{n} w_{ij}^1 \, x_j + w_{0i}\right) \tag{6}$$

where w_{0i} represents the bias for the i-th hidden neuron, and w_{ij}^1 refers to the weight connecting the input x_j to the i-th hidden neuron.

A standard approach to obtain the optimal structure of the ANN (i.e., $\boldsymbol{w} \in \mathbb{R}^{\boldsymbol{Q}}$, Q=total number of network parameters) is via the error backpropagation technique. This technique which is an approximate steepest descent (SD) algorithm is used to train the network with the following update rule

$$\boldsymbol{w_{k+1}} = \boldsymbol{w_k} - \delta g_k \tag{7}$$

where $\delta \in (0,1]$ refers to the learning rate, and g_k is the gradient evaluated at the previous guess $\boldsymbol{w_k}$, i.e.

$$g_k =: \nabla E(\boldsymbol{w})|_{\boldsymbol{w}=\boldsymbol{w_k}} \tag{8}$$

with $E(\boldsymbol{w})$ being the performance index given by the sum-of-squared error (SSE):

$$E(\boldsymbol{w}) = \frac{1}{2}\sum_{i=1}^{Q} \|e_i\|^2; \quad e_i = \tau_{a,i} - \tau_{nn,i} \tag{9}$$

where $(\tau_{a,i}, \tau_{nn,i})$ denotes the *i*-th actual-desired output pair. This work will compare three types of training algorithms; which are Gradient Descent with Momentum and Adaptive learning rate (GDMA)[15], Levenberg-Marquardt (LM)[16], and Bayesian Regularization (BR)[17].

D. Design of Experiment

The collision risk judgment for the subject is designed such that TTC can be accurately predicted when the obstacle is moving towards the subject in its heading direction, i.e., at $\theta = 0°$; and the obstacle is moving towards the subject with a trajectory non-parallel to the subject's heading direction. For performance evaluation, a video camera with MATLAB software was used to measure the actual TTC, τ_a.

The number of datasets recorded for each θ was 180, which resulted in 900 datasets in total. To evaluate the generalization capability of the proposed ANN models, the datasets were partitioned into training and test sets with a 9:1 ratio. The performance was evaluated based on the Root Mean Squared Error (RMSE), i.e.

$$\mathrm{RMSE} = \sqrt{\frac{1}{N}\sum_{i=1}^{N} e_i^2}\,;\;\; e_i = \tau_i - \tau_{di} \qquad (18)$$

With N representing the total number of test data. To measure how strong the relationship between the predicted and actual TTCs is, another performance metric which is the coefficient of determination, i.e.

$$R^2 = 1 - \frac{E_{ss}}{E_t} \qquad (19)$$

was used where E_{ss} is the sum-of-squared error, and E_t is the total sum-of-squared. In order to identify the effectiveness of the proposed ANN model, the performance was also compared with the LR method, which is a special case of ANN without the hidden layer.

III. Results

This section presents the performance evaluations on the TTC prediction method with ANN which will then be compared against the results from LR method as well as the conventional method as in (3). With regard to the ANN, two types of input features were considered, i.e., $x = x_1$ where $x_1 = \tau_x$ and $x = (x_1, x_2)$ where $x_2 = \hat{r}$. Figs. 5 and 6 depict the corresponding RMSE and R^2 from the TTC predictions based on the ANN method. The RMSE and R^2resulting from the GDMA-, LM- and BR-based models are represented by the yellow, maroon and blue lines respectively. The lowest value among all recorded RMSE for each x is denoted by the labeled marker. From the figures, the GDMA-based models do not show any clear trend across x as well as across the number of hidden neurons (i.e., q). The LM- and BR-based models on the other hand illustrate the increase in performance when q gets larger. It is also evident that both LM- and BR-based models outperformed the GDMA-based model for each x.

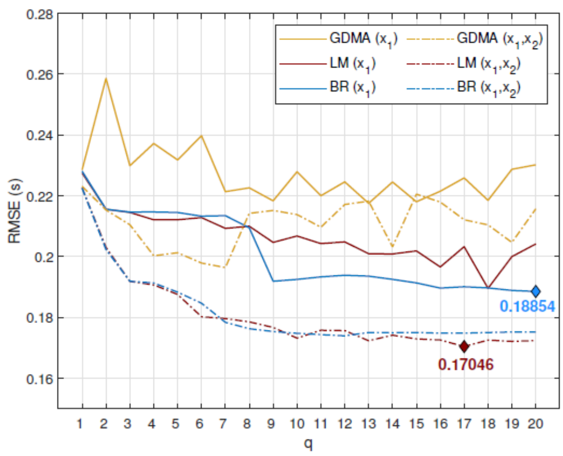

Figure 5. RMSE against the hidden layer size, q for each training algorithm. The lowest RMSE for each type of x is denoted by the labelled marker.

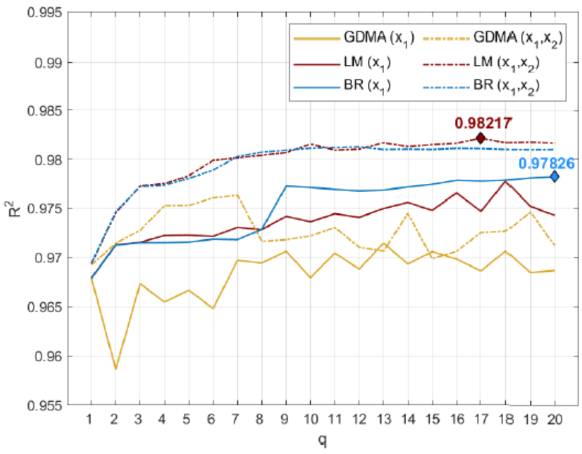

Figure 6. Coefficient of determination, R^2, against the hidden layer size, q for each training algorithm. The highest value of R^2 for each type of x is denoted by the labeled marker.

Comparing the performance between different input features, a notable trend can be observed from LM and BR methods where the average error when $x = (x_1, x_2)$ is relatively lower than those when $x = x_1$. When both parameters (i.e., τ_x and $\hat{r}$) are considered as the ANN's input features, a considerable error reduction can be achieved with the LM-based prediction giving the best performance as represented by the red plots where R^2 is 0.9852 and RMSE is only 0.155s.

Table I records the lowest RMSE and its corresponding q and R^2 for each method considered. From both Figs. 5-6 and Table I, the most significant error reduction can be obtained when $x = (x_1, x_2)$ via the LM-based model which is 50%, followed by BR- and GDMA-based models. This signifies that both data from the radar and proximity sensors are equally crucial to enhance the accuracy of the prediction.

TABLE I. Numerical Results from the TTC Prediction Methods with LR, ANN, and the Conventional Method. For the LR- and ANN-Based Prediction Methods, the Recorded Values Refer to the Lowest RMSE and Its Corresponding q and R^2 for Each x

	Input, x					
	$x = x_1$			$x = (x_1, x_2)$		
Method	**q**	**RMSE**	R^2	**q**	**RMSE**	R^2
Conventional	-	0.3103	0.95	-	-	-
LR	-	0.2698	0.946	-	0.2644	0.9577
ANN (GDMA)	13	0.2175	0.97	5	0.1740	0.9812
ANN (LM)	18	0.1896	0.98	16	0.1553	0.9852
ANN (BR)	19	0.1885	0.98	19	0.1555	0.9851

In order to observe the performance difference between the TTC prediction using the conventional method and the best methods from LR and ANN, the squared error, which is used to penalize the large error or outliers is plotted against θ as shown in Fig. 7. Despite the improvement seen from the LR-based prediction (i.e., via comparison between the top and middle plots), a number of outlier errors can still be seen particularly when $\theta = 70°$; and $\theta = 35°$. Interestingly, most errors were greatly suppressed via the ANN method as depicted in the bottom plot. A similar trend follows when the squared error is plotted against the actual TTC as visualized in Fig. 8 where the errors from the ANN method are kept close to zero across all τ_a.

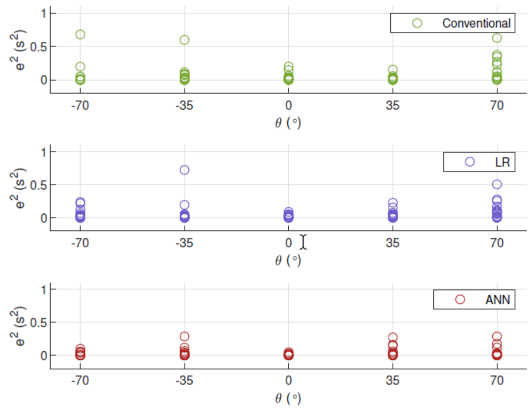

Figure 7. Squared error against angle, θ from the TTC prediction with the conventional method (top) and the best methods from LR (middle) and ANN (bottom).

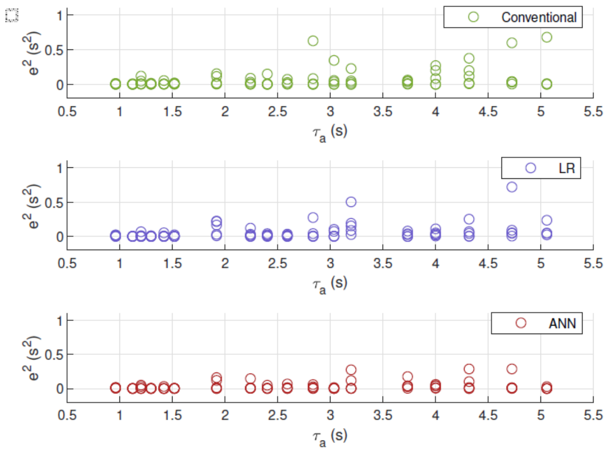

Figure 8. Squared error against actual TTC, τ_a, from the TTC prediction with the conventional method (top) and the best methods from LR (middle) and ANN (bottom).

Table II presents the average error magnitude for each method according to actual TTC intervals where lower TTC values correspond to a higher probability of collisions. Although there is no significant trend that can be observed when the errors are evaluated across the intervals, the ANN method consistently outperforms the other two methods for each interval where the average error for the most crucial interval (i.e. (0.8,2]) is only 0.1651s, which is 64.4% reduction from the conventional TTC prediction method.

TABLE II. AVERAGE ERROR MAGNITUDE FOR EACH METHOD ACROSS ACTUAL TTC INTERVALS

	Actual TTC, τ_a intervals (s)			
Method	$(\mathbf{0.8, 2}]$	$(\mathbf{2, 3}]$	$(\mathbf{3, 4}]$	$(\mathbf{4, 5}]$
Conventional	0.4647	0.3749	0.2575	0.2545
LR	0.2837	0.1306	0.1300	0.0557
ANN	0.1651	0.1117	0.0543	0.0337

IV. CONCLUSION AND FUTURE WORKS

This study has established a TTC prediction method for an AR using a Doppler radar and proximity sensors suitable for collision avoidance with an incoming obstacle. The comparative analysis has demonstrated that the ANN model trained with the LM algorithm is able to significantly reduce the error compared to those trained with BR and GDMA as well as models based on LR and conventional methods.

To further enhance the collision risk judgement technique, future work will focus on applying other machine learning methods such as Gaussian process models and projecting the TTC rate to determine the direction of multiple moving obstacles. An intelligent image sensor can also be included in the perception system to alert the subject on obstacles with the highest risk of impact during conflict occurrences.

CONFLICT OF INTEREST

The authors declare no conflict of interest.

AUTHOR CONTRIBUTIONS

All authors conducted the research, I. Arrouch, conducted the experiments; I. Arrouch and N. S. Ahmad analyzed the data; I. Arrouch wrote the paper; N. S. Ahmad, P. Goh, and J. M. Saleh validated the results; N. S. Ahmad supervised the project; all authors had approved the final version.

ACKNOWLEDGMENT

The authors would like to thank Universiti Sains Malaysia for the financial support under Research University (RUI) Grant (1001/PELECT/8014104).

REFERENCES

[1] A. Loganathan, N. S. Ahmad, and P. Goh, “Self-adaptive filtering approach for improved indoor localization of a mobile node with Zigbee-based RSSI and odometry,” *Sensors*, vol. 19, no. 21, 4748, 2019.

[2] J. H. Teo, A. Loganathan, P. Goh, and N. S. Ahmad, “Autonomous mobile robot navigation via RFID signal strength sensing,” *International Journal of Mechanical Engineering and Robotics Research*, pp. 1140–1144, 01 2020.

[3] N. S. Ahmad, “Robust H∞-fuzzy logic control for enhanced tracking performance of a wheeled mobile robot in the presence of uncertain nonlinear perturbations,” *Sensors*, vol. 20, no. 13, pp. 1–27, 2020.

[4] F. Rosique, P. J. Navarro, C. S. Fern ́andez, and A. Padilla, “A systematic review of perception system and simulators for autonomous vehicles research,” *Sensors*, vol. 19, no. 3, 2019.

[5] N. S. Ahmad, N. L. Boon, and P. Goh, “Multi-sensor obstacle detection system via model-based state-feedback control in smart cane design for the visually challenged,” *IEEE Access*, vol. 6, pp. 64182–64192, 2018.

[6] X. Yu and M. Marinov, “A study on recent developments and issues with obstacle detection systems for automated vehicles,” *Sustainability*, vol. 12, no. 8, 2020.

[7] M. Gabella, R. Notarpietro, S. Bertoldo, A. Prato, C. Lucianaz, O. Rorato, M. Allegretti, and G. Perona, “A network of portable, low-cost, x-band radars,” Joan Bech and Jorge Luis Chau, editors, in *Doppler Radar Observations*, chapter 7. IntechOpen, Rijeka, 2012.

[8] S. Kemkemian, M. Nouvel-Fiani, P. Cornic, P. L. Bihan, and P. Garrec, “Radar systems for “sense and avoid” on UAV,” in *Proc.*

2009 International Radar Conference" Surveillance for a Safer World" (RADAR 2009), 2009, pp. 1–6.

[9] S. Kingsley, *Understanding Radar Systems, Radar, Sonar & Navigation*, Institution of Engineering and Technology, 1999.

[10] Q. Fu and S. Yue, "Complementary visual neuronal systems model for collision sensing," 09 2020.

[11] R. Z. and S. Cao, "Extending reliability of mmWave radar tracking and detection via fusion with camera," *IEEE Access*, pp: 1–1, 09 2019.

[12] J. Choo, N. S. Ahmad, and P. Goh, "Autonomous navigation via visual servoing with a hybrid sensor system," *International Journal of Mechanical Engineering and Robotics Research*, pp. 906–910, 01 2020.

[13] H. Fernandes, P. Costa, V. Filipe, H. Paredes, and J. Barroso, "A review of assistive spatial orientation and navigation technologies for the visually impaired," *Universal Access in the Information Society*, 18, 03 2019.

[14] N. Long, K. Wang, R. Cheng, H. Weijian, and K. Yang, "Unifying obstacle detection, recognition, and fusion based on millimetre-wave radar and rgb-depth sensors for the visually impaired," *Review of Scientific Instruments*, 90:044102, 04 2019.

[15] T. P. Vogl, J. K. Mangis, A. K. Rigler, W. T. Zink, and D. L. Alkon, "Accelerating the convergence of the back-propagation method," *Biol. Cybern*., vol. 59, no. (4–5), pp. 257–263, September 1988.

[16] M. T. Hagan and M. B. Menhaj, "Training feedforward networks with the Marquardt algorithm," *IEEE Transactions on Neural Networks*, vol. 5, no. 6, pp. 989–993, 1994.

[17] D. MacKay, "Bayesian interpolation," *Neural Computation*, vol. 4, pp. 415–447, 1991.

Imane Arrouch was born in Agadir, Morocco. She is currently pursuing a full-time M.Sc. degree in electrical and electronic engineering with University Sains Malaysia. Her areas of interest include AI, machine learning, remote sensing and robotics.

Junita Mohamad-Saleh received her B.Sc (in Computer Engineering) from the Case Western Reserve University, USA in 1994, M.Sc. degree from the University of Sheffield, UK in 1996 and Ph.D. degree from the University of Leeds, UK in 2002. She is currently an Associate Professor at the School of Electrical & Electronic Engineering, Universiti Sains Malaysia. Her main research interest is in the area of computational intelligence (theory and applications).

Patrick Goh received the B.S., M.S., and Ph.D. degrees in electrical engineering from the University of Illinois at Urbana–Champaign, Champaign, IL, USA in 2007, 2009, and 2012 respectively. Since 2012, he has been with the School of Electrical and Electronic Engineering, Universiti Sains Malaysia, where he currently specializes in the study of signal integrity for high-speed digital designs. His research interest includes the development of circuit simulation algorithms for computer-aided design tools. He was a recipient of the Raj Mittra Award in 2012 and the Harold L. Olesen Award in 2010, and has served on the technical program committee and international program committee in various IEEE and non-IEEE conferences around the world.

Nur Syazreen Ahmad received the B.Eng. (Hons) degree in electrical and electronic engineering and the Ph.D. degree in control systems from The University of Manchester, United Kingdom, in 2009 and 2012, respectively. She is currently an Associate Professor at the School of Electrical & Electronic Engineering, Universiti Sains Malaysia, specializing in embedded control systems, mobile robotics, and sensor networks. Her research interests include intelligent control, robust constrained control, autonomous mobile systems, and brain-computer interface.